



1 **The temperature-dependent shear strength of ice-filled**
2 **joints in rock mass considering the effect of joint**
3 **roughness, opening and shear rates**

4 Shibing Huang^{1,2}, Haowei Cai¹, Zekun Xin¹, Gang Liu¹

5 ¹ School of Resources and Environmental Engineering, Wuhan University of Science and Technology,
6 Wuhan, Hubei 430081, China

7 ² Hubei Key Laboratory for Efficient Utilization and Agglomeration of Metallurgic Mineral Resources,
8 Wuhan University of Science and Technology, Wuhan, Hubei 430081, China

9 *Correspondence to:* Shibing Huang (huangshibing@wust.edu.cn)

10 **Abstract.** Global warming causes many rockfall activities of the alpine mountains, especially when ice-
11 filled joints in the rock mass become thawed. The warming and thawing of frozen soils and intact rocks
12 was widely studied in the past several decades, however, the variation of shear strengths of ice-filled
13 joints was not fully understood. Recently, some scholars studied the thawing process and strength loss
14 of ice-filled joints at different temperatures, however, the influence of the joint roughness, opening and
15 shear rate on ice-filled joints was not systematically investigated. In this study, a series of compression-
16 shear experiments were conducted to investigate the shear strength of ice-filled rock joints by considering
17 the effects of joint roughness, opening and shear rates. The shear strength quickly reduces with increasing
18 temperature, especially above -1 °C. In addition, the shear strength decreases with increasing joint
19 openings but it increases with increasing joint roughness. When the joint opening is large enough, the
20 effect of joint roughness disappears and the shear strength of ice-filled joints is equal to that of solid ice.



21 Increasing shear rate will decrease the shear strength of ice-filled joints because the joint ice displays the
22 brittle failure phenomenon at a high shear rate. The Mohr-coulomb criterion also can be used to
23 characterize the relationship between the shear strength and the normal stress of ice-filled joints.
24 However, a general strength model by considering the joint opening, normal stress and joint roughness
25 should be proposed by a further study. This research can provide a better understanding of the warming
26 degradation mechanism of ice-filled joints by considering the above important influencing factors.

27 **1 Introduction**

28 With the increase of global temperature and human activities in permafrost areas, many alpine rock
29 masses become more unstable (Gruber and Haerberli, 2007; Allen and Huggie, 2013; Hartmeyer et al.,
30 2020; Legay et al., 2021; Hilger et al., 2021). A large number of rockfalls in permafrost alpine bedrock
31 slopes indicated the exposure of broken ice after shear failure, which could cause serious natural
32 geological disasters (Krautblatter et al., 2021; Walter et al., 2019). For example, the rockfall disaster that
33 happened in Chamoli, Indian Himalaya, in 2021 took more than 200 lives and destroyed two hydropower
34 facilities (Shugar et al., 2021). According to investigation results, this rockfall disaster was caused by the
35 warming and thawing of ice. Although the freezing expansion process of joint ice was harmful for the
36 stability of joint rock masses, the bonding strength between ice and joint wall can strengthen the joints
37 themselves after complete freezing (Matsuoka and Murton, 2008; Zhang et al., 2020; Shan et al., 2021).
38 However, if the joint ice was thawed, the rock-ice-rock “sandwich” structure would be debonded and
39 unstable. In addition, the liquid water produced by warming ice could lower the friction between joint
40 surface and thus reduced the stability of joint rock slopes (Zhao et al., 2017). Many field data showed
41 that most of the irreversible fracture displacement and rockfall happened in the warm seasons instead of



42 the cool seasons because the warming and thawing of joint ice could greatly decrease the strength of rock
43 mass containing ice-filled joints (Weber et al., 2018; Etzelmüller et al., 2022). Yang et al. (2019) claimed
44 that the existence of detached ice block could promote the mobility of ice-rock system and thus cause a
45 more serious geological disaster on alpine rock slope. Therefore, the warming degradation of the ice-
46 rock interface and the strength loss of ice-filled joints should be comprehensively studied.

47 In the past decades, the warming degradation of permafrost soils was widely investigated, however, there
48 is little literature reporting the strength loss of rocks containing ice-filled joints. The shear experiment of
49 the ice-rock interface might be first conducted by replacing the rock with concrete in order to make a
50 specific roughness (Davies et al., 2001, 2017). These experiments were conducted at the temperature
51 from -5 to 0 °C. Krautblatter et al. (2012) developed a shear strength model for the ice-filled joints that
52 incorporates the cracking of rock bridges, the friction of rough joint walls, creep of ice and detachment
53 of rock-ice interfaces. Mamot et al. (2018) conducted a systematic study of the shear failure of limestone-
54 ice and mica-rich interfaces at constant strain rates from -10 to -0.5°C, and they found that the normal
55 stress and freezing temperature were two important factors influencing the shear strength. However, the
56 uniform joint surfaces were used without considering the influence of joint roughness. Mamot et al. (2021)
57 further predicted the warming stability of permafrost slopes containing ice-filled joints by using the
58 Universal Distinct Element Code (UDEC). The simulation results verified that the warming temperature
59 close to the melting point might drive the slide of a slope with angle of 50°-62°, and the actual slope
60 angle also depended on the joint orientation. The above research mainly investigated the thawing
61 temperature and normal stress on the shear strength of ice-filled joints. The highest normal stress is about
62 1.438 MPa (Davies et al., 2001), and the maximum range for the temperature was -10 °C to -0.5 °C



63 (Mamot et al., 2018). However, the freezing depth could exceed 100 m for some alpine caves containing
64 frozen ice (normal stress large than 2 MPa) and the temperature was less than -15 °C as observed in the
65 field (Colucci and Guglielmin, 2019). Therefore, a much wider range of temperature and normal stress
66 should be considered when investigating the shear characteristics of ice-filled joints.

67 In addition, although some scholars began to pay attention to the mechanical properties of ice-filled joint
68 rock mass, the influence of many important factors on the shear strength of ice-filled joints was not
69 investigated, including the joint roughness, shear rate, normal stress and joint opening. Generally, the
70 natural joints have different roughness and openings (Shen et al., 2020). In this study, a comprehensive
71 shear experiment was performed on the ice-filled joints in sandstones. The main purpose was to reveal
72 the influencing mechanism of freezing temperature, joint roughness, shear rate, joint opening and normal
73 stress on the shear strength of ice-filled joints in rock masses. This research can provide a better
74 understanding of the warming degradation process of the ice-filled joints and the thawing disaster of
75 alpine mountains in cold regions.

76 **2 Materials and methods**

77 **2.1 Collection of sandstones**

78 The red sandstones collected from Yichang city of Hubei province were used in this experiment. This is
79 a typical sedimentary rock and is widely distributed on the surface of the earth. The block samples with
80 approximately equal P-wave (compressional wave) velocities were chosen to make frozen samples
81 containing ice-filled joints. The basic physico-mechanical properties of this red sandstone are given in
82 Table 1.



83 **Table 1.** The basic physico-mechanical properties of the fresh sandstone. ρ : density. n : porosity. V_p : primary.
84 wave velocity. τ_{ps} : shear strength. UCS: uniaxial compressive strength.

ρ (g/cm ³)	n (%)	V_p (m/s)		τ_{ps} (MPa)		UCS (MPa)	
		Dry	Saturated	Dry	Saturated	Dry	Saturated
2.32	7.71	2992	3264	7.60	3.02	79.53	30.97

85

86 2.2 Preparation of ice-filled joint rock mass

87 According to the JRC index proposed by Barton and Choubey (1977), five kinds of roughness were used
88 in this experiment, including No. 2 (2°-4°), No. 4 (6°-8°), No. 6 (10°-12°), No. 8 (14°-16°) and No. 10
89 (18°-20°), respectively. The frozen samples containing ice-filled joints are made in the laboratory
90 because it is hard to cut or drill them in the fields. The manufacturing process of ice-filled joint rock mass
91 mainly includes the following steps:

92 ① The original rock blocks were cut into the designed rectangular blocks (100 mm × 100 mm × 50
93 mm) by using a rock cutting machine.

94 ② These rectangular blocks were used to engrave different rough curves on the surface by using a 3D
95 numerical control engraving machine. The roughness can be controlled by implanting the standard JRC
96 curves into the controlling system of this machine. Each frozen rock sample containing an ice-filled joint
97 was assembled by using a pair of rectangular blocks with the same roughness.

98 ③ The rock blocks were heated in a dry oven at 105 °C in order to tightly paste the waterproof tape
99 and prevent the escape of joint water during freezing.



100 ④ The joint opening was divided into different specified thicknesses which were controlled by
 101 inserting rubber strips, and a piece of waterproof tape was pasted on the surface in order to store water.
 102 ⑤ When the waterproof tape was tightly bonded on the rock surface, liquid water should be injected
 103 into the artificial joint until no water leaks out. After that, the water-filled joint rock mass was put into a
 104 steel mold to freeze in a freezing chamber. The steel mold was used to control the joint opening because
 105 the volume of joint water would expand during freezing. Then ice-filled joint samples can be derived
 106 after freezing at $-20\text{ }^{\circ}\text{C}$ for 12 h. The manufacturing procedure and related ice-filled joint samples were
 107 shown in Fig. 1.

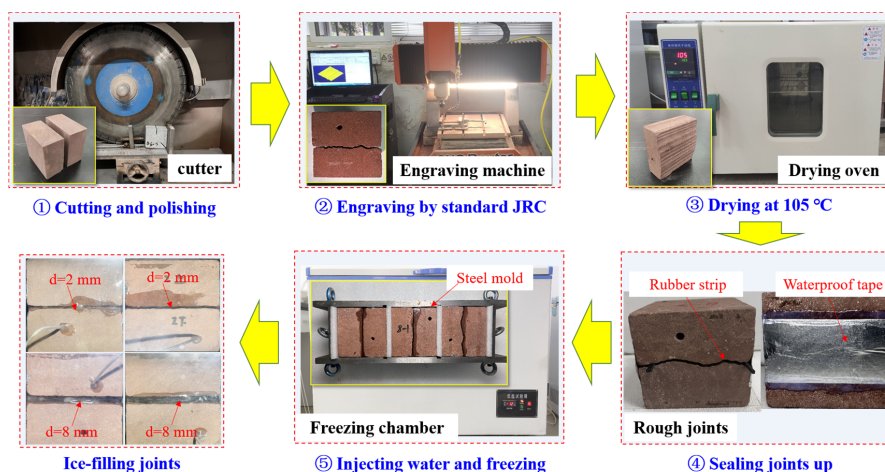
108 **Table 2.** Ten standard joint profiles (Barton and Choubey, 1977).

Profile No.	Typical roughness profiles	JRC range
No. 1		0-2 (0.4)
No. 2		2-4 (2.8)
No. 3		4-6 (5.8)
No. 4		6-8 (6.7)
No. 5		8-10 (9.5)
No. 6		10-12 (10.8)
No. 7		12-14 (12.8)
No. 8		14-16 (14.5)



No. 9		16-18 (16.7)
No. 10		18-20 (18.7)

109



110

111 **Figure 1.** Preparation of ice-filled joints. The preparation steps are as follows: ① Cutting and polishing, ②
 112 Engraving by standard, ③ Drying at 105 °C, ④ Sealing joints up, ⑤ Injecting water and freezing.

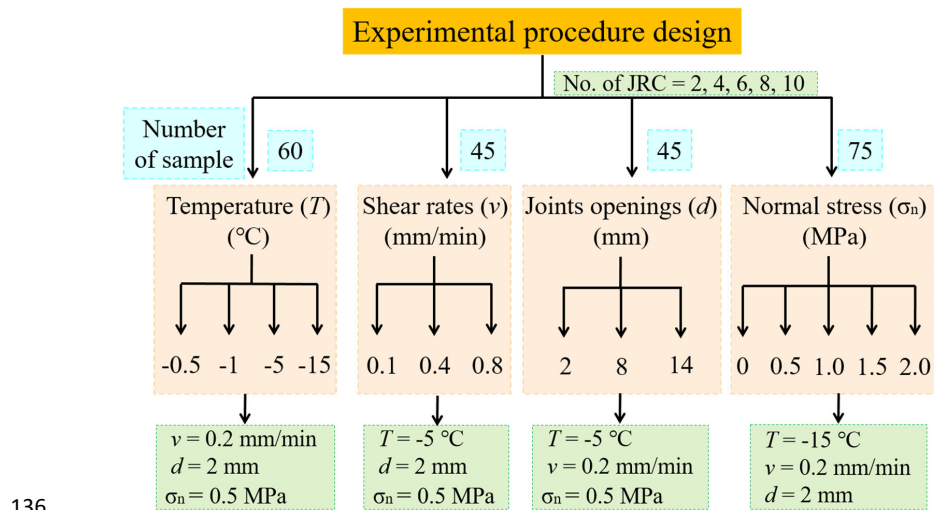
113 **2.3 Experimental procedures**

114 The main objective of this study is to investigate the effect of critical factors on the shear strength of ice-
 115 filled joint rock mass, including the freezing temperature, joint roughness, shear rates, joint opening and
 116 normal stress. The joint roughness is a basic index for rock joints, which is always considered when
 117 investigating other factors. Therefore, all the samples can be divided into 4 groups, namely the
 118 temperature group, shear rate group, joint opening group, and normal stress group. In the pre-test, the
 119 shear strength of the ice-filled joint does not change when the temperature is below -5 °C, however, it
 120 greatly decreases when the temperature increases from -5 °C to 0 °C. Therefore, the temperatures are set



121 as $-15\text{ }^{\circ}\text{C}$, $-5\text{ }^{\circ}\text{C}$, $-1\text{ }^{\circ}\text{C}$ and $-0.5\text{ }^{\circ}\text{C}$, respectively. The shear rates are 0.2 mm/min , 0.4mm/min and
122 0.8mm/min in the shear rate group. In the joint opening group, the openings of ice-filled joints are 2 mm ,
123 8 mm and 14 mm , respectively. The freezing depth on the earth may be small, however, it can exceed
124 100 m in some alpine caves, where the in-situ stress is close to 2 MPa . Therefore, in the normal stress
125 group, the normal stresses are set as 0 MPa , 0.5 MPa , 1 MPa , 1.5 MPa and 2 MPa , respectively. Three
126 parallel experiments were performed on each group to eliminate the discreteness of ice-filled joint
127 samples and experiment error. There are approximately 225 ice-filled joint samples prepared in this
128 experiment. The distribution of these ice-filled joint samples were shown in Fig. 2.

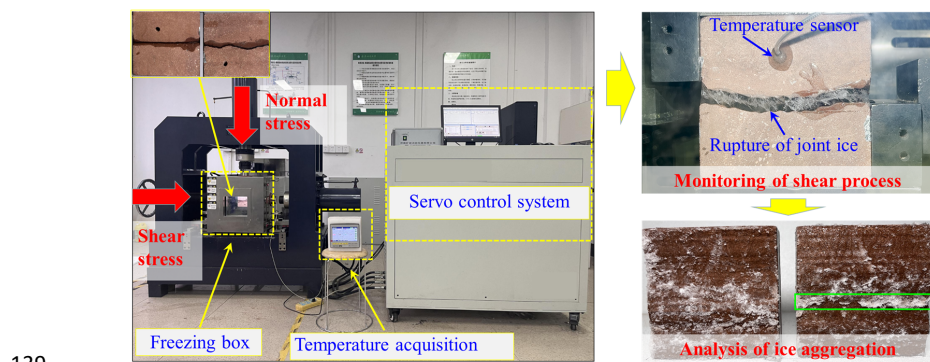
129 All the water-containing joints were frozen in a freeze box at a specific temperature for about 12 h, and
130 they were used to conduct the direct shear experiment on a temperature-controlled shearing instrument
131 under the scheduled low temperature and normal stress. A temperature sensor was implanted into the
132 sample to accurately monitor the internal temperature change of ice-filled joint samples. When the
133 scheduled freezing temperature was reached, the normal stress was applied with a loading rate of 0.2
134 kN/s . Then the shear process was performed in the displacement mode with the designed shear rate. After
135 the shear experiment, the rupture modes of ice-filled joints were captured and analyzed by using a camera.



136

137 **Figure 2.** Distribution of rock samples containing ice-filled joints. T : Temperature. v : Shear rates. d : Joint openings.

138 σ_n : Normal stress.



139

140 **Figure 3.** Shear experiment procedure and equipment



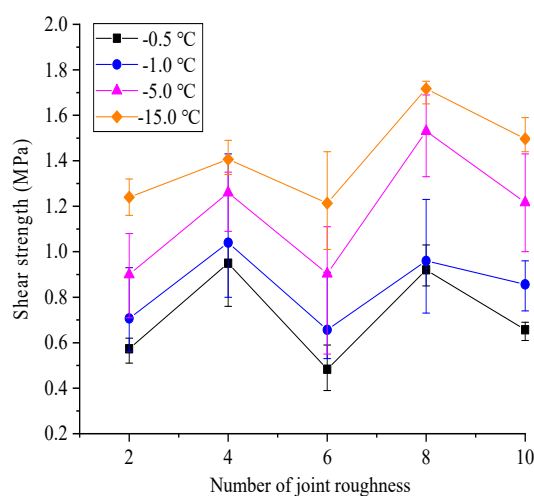
141 **3 Experimental results**

142 **3.1 Effect of freezing temperature and joint roughness**

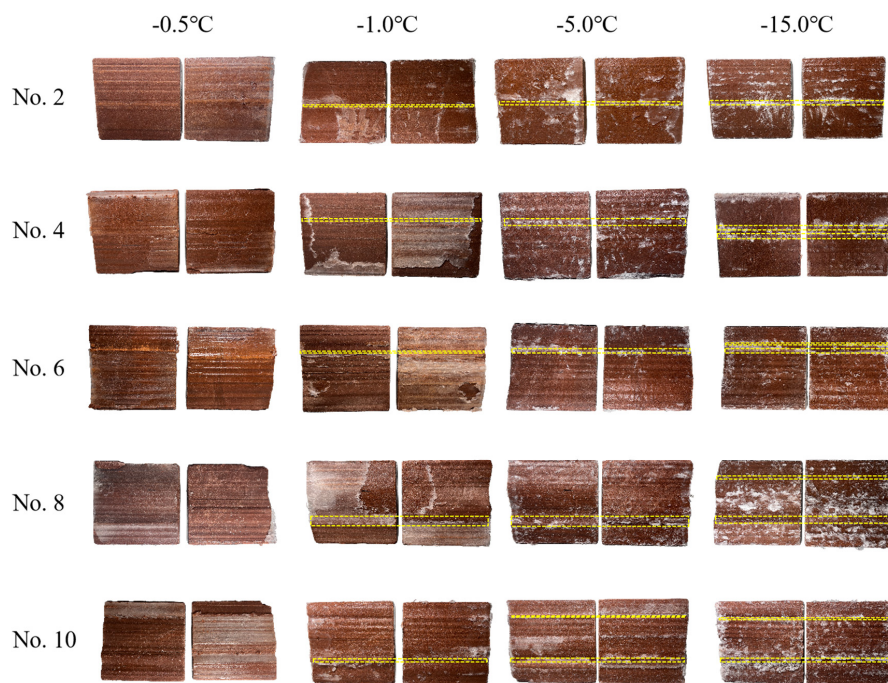
143 In the temperature group, freezing temperatures were set as $-15\text{ }^{\circ}\text{C}$, $-5\text{ }^{\circ}\text{C}$, $-1\text{ }^{\circ}\text{C}$ and $-0.5\text{ }^{\circ}\text{C}$, and the joint
144 roughness was named by the profile number in Table 2. The shear strength is dependent on the freezing
145 temperature and joint roughness as shown in Fig. 4. The shear strength decreases remarkably with
146 increasing freezing temperature. When the temperature increases from $-15\text{ }^{\circ}\text{C}$ to $-0.5\text{ }^{\circ}\text{C}$, the mean
147 strength decreases by approximately 54%, 32%, 60%, 46% and 56% for profiles of No. 2, No. 4, No. 6,
148 No. 8 and No. 10, respectively. The shear strength of ice-filled joints does not always increase with JRC,
149 which has a considerable reduction at the joint profiles of No. 6 and No. 10. It illustrates that solid ice is
150 a kind of special infilling material, which is different from soft soils or cement-based materials. The
151 change law of shear strength against JRC may be explained by the shear rupture mode as shown in Fig.
152 5. There are several aggregation regions of rupture ice close to large climbing bulges on the surface of
153 joints. The peak shear strength of ice-filled joints is related to the aggregation area of rupture ice; because
154 a large shear force is required to promote the solid ice to shear slide along the slope of bulges. The
155 aggregation area and location along the rough profile of joints after shear failure are plotted in Fig. 6. It
156 can be observed that the aggregation ice appears before several high bulges and the aggregation location
157 is almost independent of the freezing temperature if aggregation ice occurs. The climbing bulges in front
158 of the aggregation ice are noticeable and influential. It implies that the influence of joint roughness on
159 the shear strengths of these ice-filled joints may be only controlled by several noticeable bulges instead
160 of the JRC index. Figure 7 shows that the shear strengths of No. 6 and No. 10 display obvious reduction
161 trends, which may be in accordance with the ice aggregation area. The ice aggregation area decreases



162 with increasing the freezing temperature, because the bonding strength between ice and joint surface
163 becomes to be weaker, and the shear rupture happens along the ice-rock interface instead of solid ice
164 when the freezing temperature is larger than $-0.5\text{ }^{\circ}\text{C}$.
165 In addition, when the freezing temperature is close to $0\text{ }^{\circ}\text{C}$, the pre-melting of ice-rock interface induced
166 by the normal stress will cause a reduction of bonding strength. Therefore, the shear strength between
167 bonded ice-rock interfaces is much smaller than the shear strength of solid ice at a high freezing
168 temperature close to the melting point of bulk ice, such as $-0.5\text{ }^{\circ}\text{C}$. It should be noted that the aggregation
169 phenomenon of rupture ice disappears when $T = -0.5\text{ }^{\circ}\text{C}$ because the high-temperature ice is ductile failure
170 along the ice-rock interface instead of the joint ice itself. However, the climbing effect still makes a
171 significant contribution to the increase of shear strength.

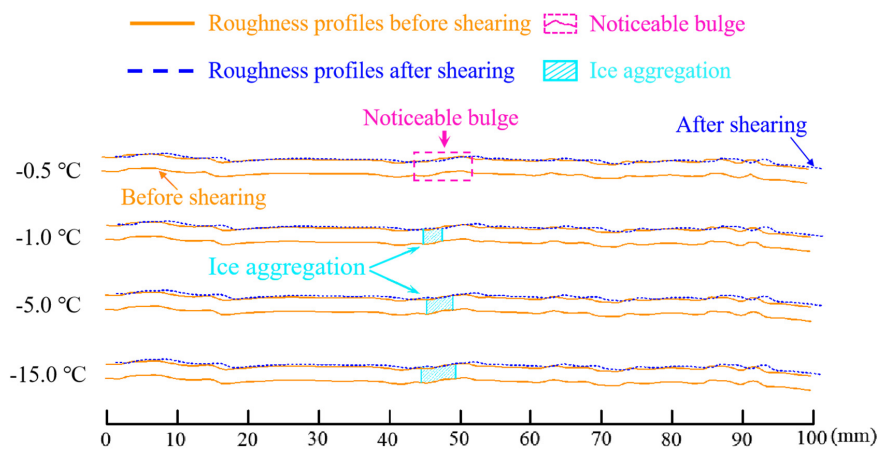


172
173 **Figure 4.** Shear strength against joint roughness at different freezing temperatures. Experimental condition: $v = 0.2$
174 mm/min , $d = 2\text{ mm}$, $\sigma_n = 0.5\text{ MPa}$.

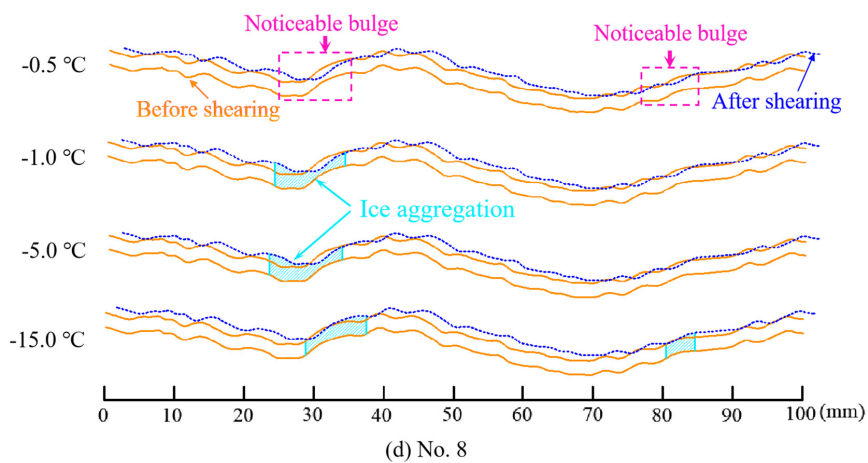
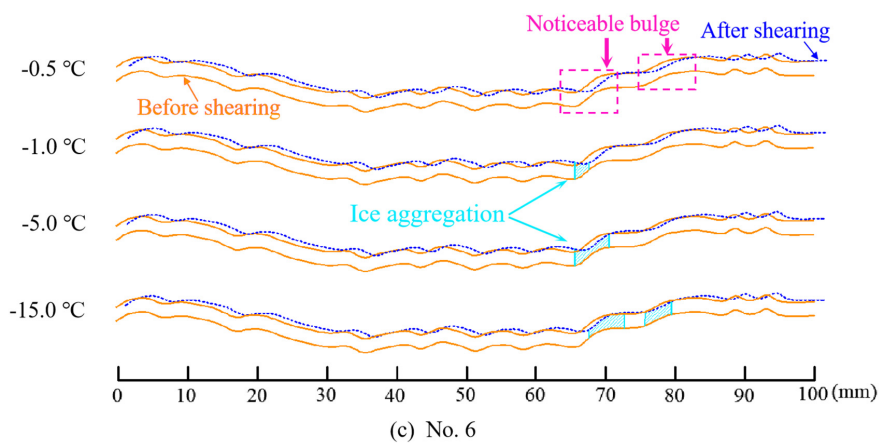
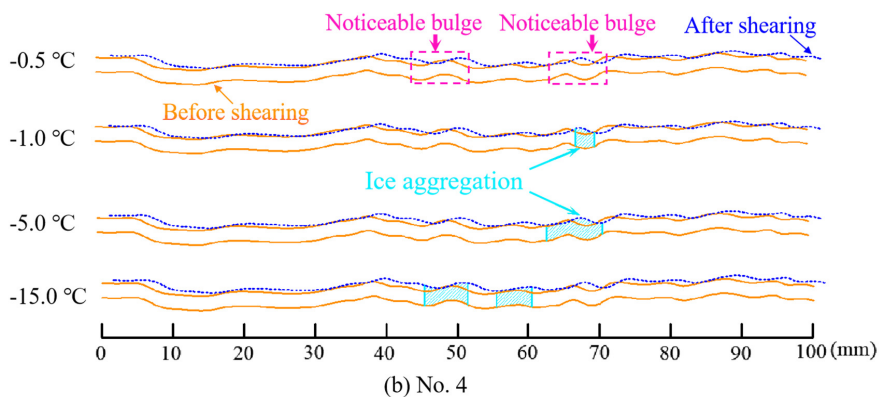


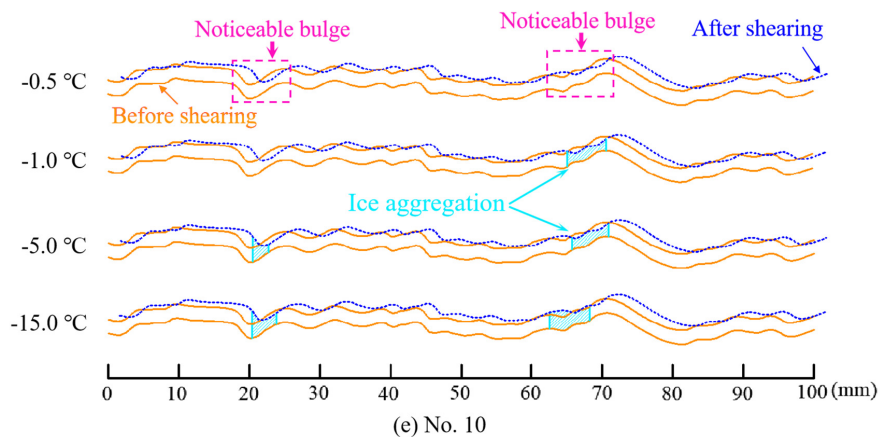
175

176 **Figure 5.** Shear rupture modes of ice-filled joints at different freezing temperatures. The yellow lines show the main
 177 aggregation of rupture ice. Ice after rupture will aggregate in roughness bulges perpendicular to the shear direction.



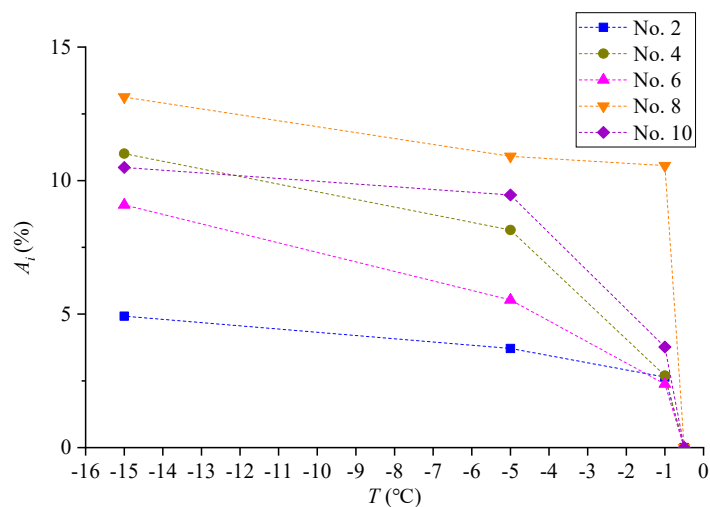
178





182

183 **Figure 6.** Shear aggregation areas of ice along the profile of roughness. Experimental condition: $v = 0.2$ mm/min, d
 184 $= 2$ mm, $\sigma_n = 0.5$ MPa. Some blue profiles are located under the orange profiles after shearing, which means the
 185 width of joints becomes smaller. Generally, the reduction of width occurs before some bulges and the rupture ice
 186 will aggregate before these bulges. These bulges are defined as noticeable bulges. Therefore, the bulges causing the
 187 reduction of joint width and aggregation of ice are called noticeable bulges in this study.



188



189 **Figure 7.** Aggregation area of rupture ice increases with the reduction of freezing temperature. Experimental
190 conditions: $v = 0.2$ mm/min, $d = 2$ mm, $\sigma_n = 0.5$ MPa. A_i : aggregation area of rupture ice.

191 The peak shear displacement and normal displacement also are dependent on the freezing temperature
192 (Table 3 and Table 4). With the increase of freezing temperature, the peak shear displacement increases
193 because the joint ice will change from brittle to ductile (Bragov et al., 2015). Ice is brittle at -15 °C and
194 -5 °C, so the maximum shear displacement before failure is small at this temperature and the shear failure
195 mode displays brittle characteristics. When the temperature increases to -1 °C, the solid ice becomes to
196 be ductile, therefore a larger shear displacement arises before failure. However, the shear dilatancy
197 reduces with increasing the freezing temperature. Solid ice is a kind of temperature-dependent material,
198 the elastic modulus of which almost linearly decreases with increasing the freezing temperature (Sinha,
199 1989; Han et al. 2016). The inhibition of normal stress on the shear dilatancy is greater at the high freezing
200 temperature during shear process.

201 Several typical shear stress-displacement and normal-shear displacement curves for the profile of No. 4
202 are plotted in Fig. 8. The ice-filled joint shows significant residual shear strength beyond the peak point,
203 which slightly decreases with increasing shear displacement. This residual shear strength is caused by
204 the friction effect between the upper and lower ice-filled blocks. In addition, the normal shear dilatancy
205 displays increasing trend with shear displacement, which is caused by the climbing effect of ice-filled
206 joints. It should be noted that the shear strength has a second rising point at the residual strength stage,
207 because the shear rate is increased from 0.2 mm/min to 1 mm/min in order to accelerate the completion
208 of the shear process. Schulson and Fortt (2012) claimed that the friction between ice interfaces increases



209 when the shear rates increase from 0.06 mm/min to 0.6 mm/min. Therefore, the sudden rise of residual
210 shear strength can be attributed to the accelerated shear rate.

211

212 **Table 3.** The peak shear displacement at the peak points of shear strength (mm)

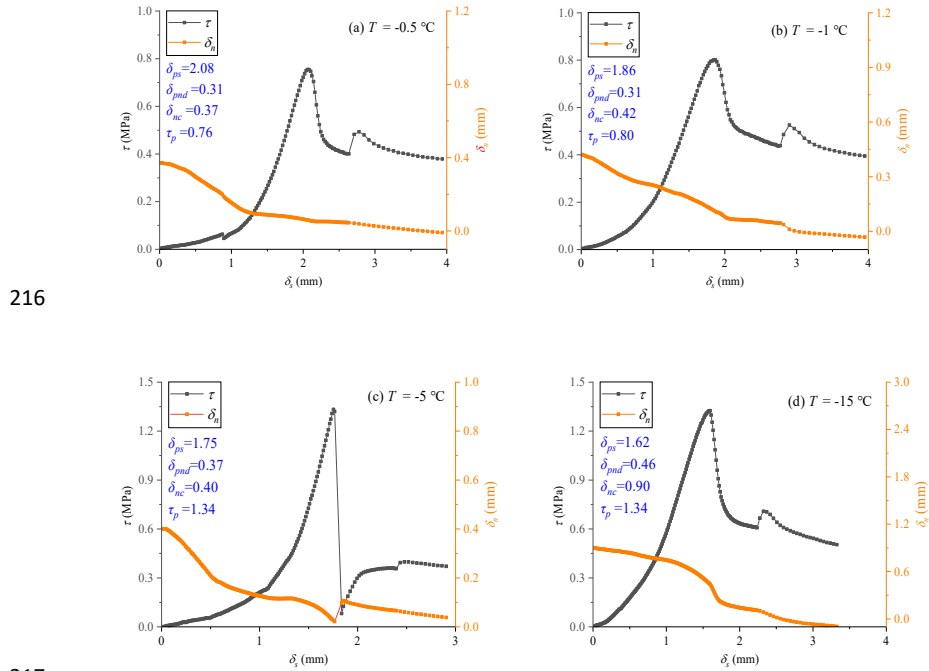
Profile No.	Freezing temperature			
	-15 °C	-5 °C	-1 °C	-0.5 °C
No. 2	1.36	1.46	1.72	1.84
No. 4	1.62	1.75	1.86	2.08
No. 6	1.33	1.53	1.71	1.83
No. 8	1.78	1.85	1.99	2.12
No. 10	1.63	1.79	1.87	1.94

213

214 **Table 4.** The normal shear dilatancy at the point of peak shear strength (mm)

Profile No.	Freezing temperature			
	-15 °C	-5 °C	-1 °C	-0.5 °C
No. 2	0.24	0.23	0.14	0.08
No. 4	0.46	0.37	0.31	0.31
No. 6	0.27	0.28	0.22	0.12
No. 8	0.77	0.44	0.37	0.36
No. 10	0.61	0.32	0.21	0.39

215



216

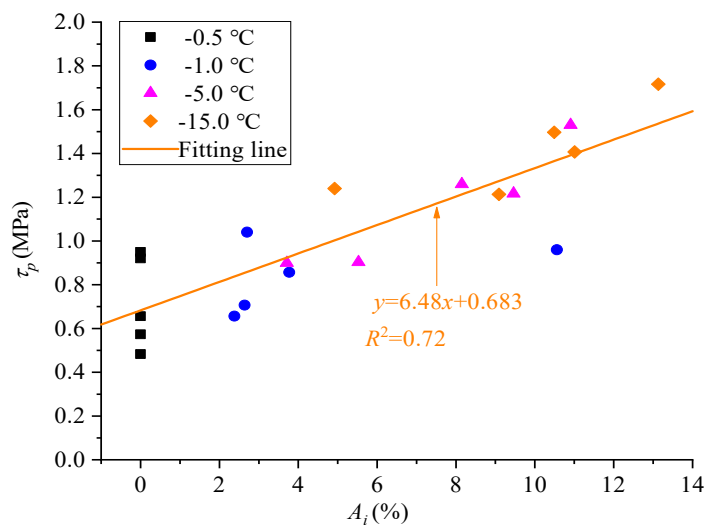
217

218 **Figure 8.** Shear strength and normal displacement versus the shear displacement for the profile of No. 4 in the
 219 temperature group. δ_{ps} and δ_{pnd} are the shear displacement and normal shear dilatancy at the point of peak shear
 220 strength, τ_p and δ_{nc} is the initial compression deformation.

221 Another finding is that the JRC is not suitable to interpret the influence of joint roughness on the shear
 222 strength of ice-filled joints, because the peak shear strength does not monotonically increase with
 223 increasing JRC index. The peak shear strength displays an increase-decrease-increase-decrease trend
 224 against JRC from No. 2 to No. 10 (Fig. 4). Figure 9 shows that the peak shear strength displays a linear
 225 increasing trend with increasing aggregation areas of fragmented ice after failure. The aggregation area
 226 of fragmented ice can be treated as the effective climbing area which makes a significant contribution to
 227 the improvement of shear strength, because the fragmented ice is produced under compression-shear



228 stress in the process of climbing the steep bulges. As a consequence, only these steep bulges causing
229 aggregation of rupture ice contribute to the improvement of shear strength. The variation law of shear
230 dilatancy against the roughness also is in accordance with the shear strength of ice-filled joints, but it is
231 different from the change law of JRC (Table 4). In Fig. 6, the gathering of fragmented ice mainly arises
232 in the front of the steepest bulge. It illustrates that the improvement of shear strength of joint ice is caused
233 by a part of the steepest bulge instead of the total roughness. Therefore, JCR may be not suitable for the
234 prediction of shear strength of ice-filled joints. For example, although the JCR of No. 6 is much larger
235 than No. 4, the effective steep bulge to cause ice aggregation after failure is smaller than that of No. 4
236 (Fig. 7). This phenomenon confirms that the improvement of shear strength is only caused by some
237 noticeable steep bulges instead of the total bulges.

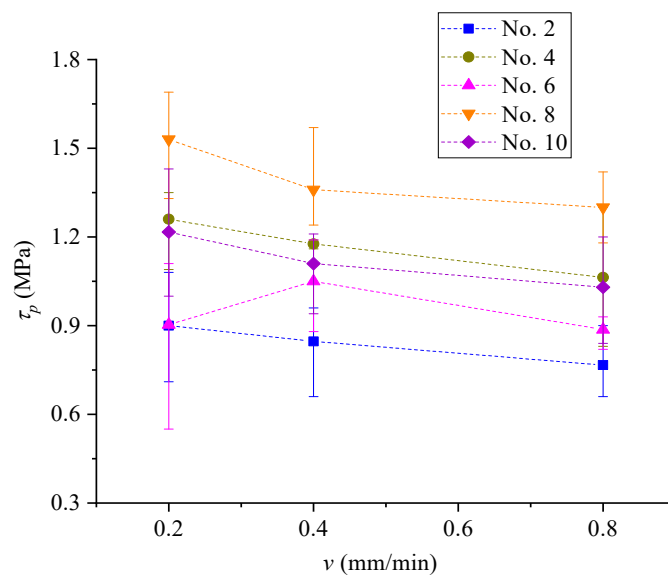


238
239 **Figure 9.** Peak shear strength linearly increases with increasing aggregation areas of rupture ice. Experimental
240 condition: $v = 0.2$ mm/min, $d = 2$ mm and $\sigma_n = 0.5$ MPa.



241 **3.2 Effect of shear rates**

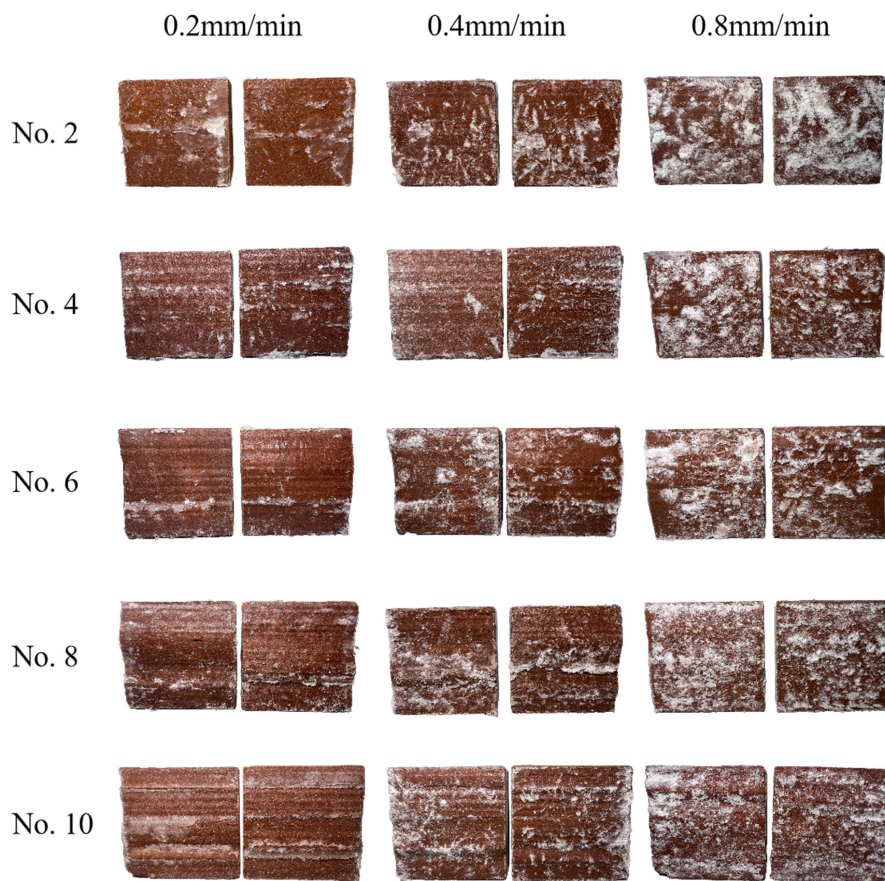
242 The shear rates have significant effects on the strength of solid ice as observed in the previous literature
243 (Petrovic, 2003). Low shear rates are used to conduct quasi-static shear experiments, including 0.2
244 mm/min, 0.4 mm/min and 0.8 mm/min. Figure 10 shows that the peak shear strength slightly decreases
245 with increasing shear rates. Solid ice is a kind of typical elasto-plastic material. When the shear rate is
246 slow, the ice crystal has enough time to shear slip and it will present ductile failure characteristics. At a
247 low shear rate, the free water on the slip interface will reorganize at the water-ice interface to form ice,
248 however, it is hard for the ice crystal to adjust to adapt the shear slip at high shear rates, which will cause
249 the shear rupture of ice crystals and hinder the growth of ice on the water-ice interface (Lou et al., 2019).
250 Figure 11 shows that a high shear rate will induce brittle failure of joint ice and more fragmented ice
251 crystals are produced. As a result, the shear strength reduces with increasing shear rates from 0.2 mm/min
252 to 0.8mm/min. The previous literature shows that there is a critical loading rate for the transition from
253 ductile to brittle behavior of polycrystalline ice (Timco and Frederking, 1982; Gold, 2018). In this study,
254 the transition point of ice-filled joint is not definitely derived due to the limitation of the shear rate range.



255

256 **Figure 10.** Effect of shear rate on the peak shear strength. Experimental condition: $T = -5$ °C, $d = 2$ mm and $\sigma_n = 0.5$

257 MPa.



258

259 **Figure 11.** The shear rupture characteristics of joint ice under different shear rates. Experimental condition: $T = -$

260 $5\text{ }^{\circ}\text{C}$, $d = 2\text{ mm}$ and $\sigma_n = 0.5\text{ MPa}$. The ice crystal that cannot adapt to shear slip at high shear rates will form brittle

261 failure. The joint ice of brittle failure shows more micro fractures which make it more reflective. This will cause a

262 white appearance of the rupture ice on the joint surface. The ductile failure of ice displays a transparent appearance

263 without white color, which is hard to observe. Therefore, a larger area of white appearance implies a much more

264 serious brittle failure of joint ice.

265



266 **3.4 Effect of joint openings**

267 Joint opening is another critical factor influencing the shear strength of ice-filled joints. The maximum
268 height difference of the standard JRC curves suggested by Barton and Choubey (1977) is approximately
269 2.14 mm, 2.40 mm, 6.24 mm, 6.85 mm and 4.48 mm for the profiles of No. 2, No. 4, No. 6, No. 8 and
270 No. 10, respectively. The joint openings are chosen as 2 mm, 8 mm and 14 mm because 2 mm is smaller
271 than all the maximum height differences while 14 mm is much larger than them. The rupture
272 characteristics of joint ice against the joint opening are plotted in Fig. 12. When the joint opening is 2
273 mm, the aggregation phenomenon of rupture ice is evident. However, the aggregation phenomenon
274 disappears for the profiles of No. 2, No. 4 and No. 6 when the joint opening is 8 mm. When the joint
275 opening increases to 14 mm, there is not any aggregation of rupture ice arising for all the joints. Figure
276 13 shows that when the joint opening increases from 2 mm to 14 mm, the shear strength of ice-filled
277 joints decreases. The shear strength of pure solid ice also is measured in the laboratory, which is
278 approximately 0.83 MPa on the condition that $T = -5\text{ }^{\circ}\text{C}$, $v = 0.2\text{ mm/min}$ and $\sigma_n = 0.5\text{ MPa}$. When the
279 joint opening is 14 mm, the shear strengths of ice-filled joint are approximately 0.83 MPa and they are
280 independent of the joint roughness. When the joint opening is 8 mm, the shear strengths of ice-filled joint
281 are very close to the shear strength of pure solid ice (0.83 MPa) for the joint of No. 2, No. 4 and No. 6.
282 The reason is that 8 mm has exceeded the critical filling thickness of these joints (No. 2, No. 4 and No.
283 6), therefore the shear strength of these ice-filled joints is only controlled by the solid ice instead of joint
284 roughness. In addition, there is not any significant ice aggregation on the joint surfaces of No. 2, No. 4
285 and No. 6 when the joint opening is 8 mm, and the shear failure happens inside the joint ice. However,
286 for the ice-filled joints of No. 8 and No. 10, the shear strengths are larger than 0.83 MPa, which illustrates



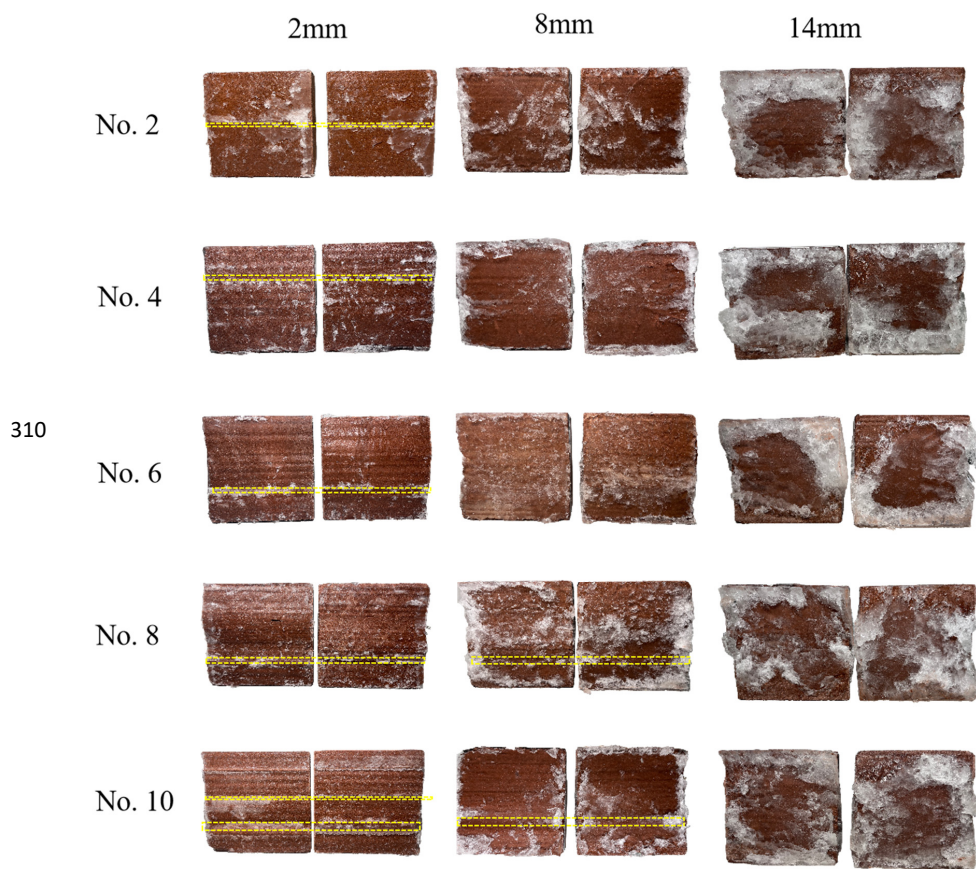
287 that the critical filling thickness for the profiles of No. 8 and No. 10 should be larger than 8 mm but
288 smaller than 14 mm. There is aggregation ice arising before large bulges, and these large bulges would
289 prevent the direct shear failure of joint ice and improve the shear strength.

290 The influence of joint opening and roughness on the shear strength can be explained by using the shear
291 failure path of ice-filled joints as shown in Fig. 14. When $d=2$ mm, the shear climbing will occur before
292 some large bulges for all the joint profiles. This climbing action induces the aggregation of rupture ice
293 and change of shear path. As a consequence, the shear strength will improve. When $d=8$ mm, the shear
294 failure path will not be disturbed for the profiles of No. 2, No. 4 and No. 6, however, the shear failure
295 path changes due to the climbing action for the profiles of No. 8 and No. 10, in which a significant
296 aggregation of rupture ice is produced. Therefore, the shear strengths of ice-filled joints for the profiles
297 of No. 2, No. 4 and No. 6 are approximately equal to the solid ice, while the shear strengths for the
298 profiles of No. 8 and No. 10 are much larger than 0.83 MPa. When $d = 14$ mm, the shear failure happens
299 inside the joint ice for all joint profiles, therefore, the shear failure path and shear strength will not be
300 influenced by the joint roughness and no aggregation of rupture ice occurs. The shear dilatancy
301 deformation of the ice-filled joints in Fig. 15 has further proved the climbing actions, including all the
302 profiles with joint opening of 2 mm, and the profiles of No. 8 and No. 10 with joint opening of 8 mm.

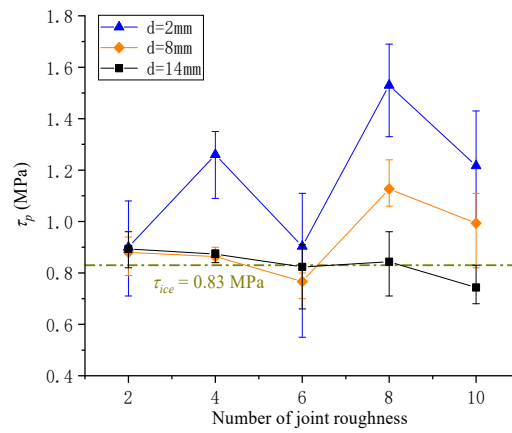
303 The climbing effect of the No. 2 ice-filled joint with opening of 2 mm is not remarkable, therefore the
304 shear dilatancy is very small and the shear strength also is close to pure solid ice (0.83 MPa). Regardless
305 of the critical filling thickness, the present study shows that the shear strength of ice-filled joints
306 decreases with increasing joint openings from 2 mm to 14 mm, and it is related to the joint roughness
307 below the critical infilling thickness. When the filling ice exceeds the critical thickness, the shear strength



308 of ice-filled joints is equal to the shear strength of solid ice under the same condition. It should be noted
309 that the critical filling thickness for each roughness will be determined in future studies.



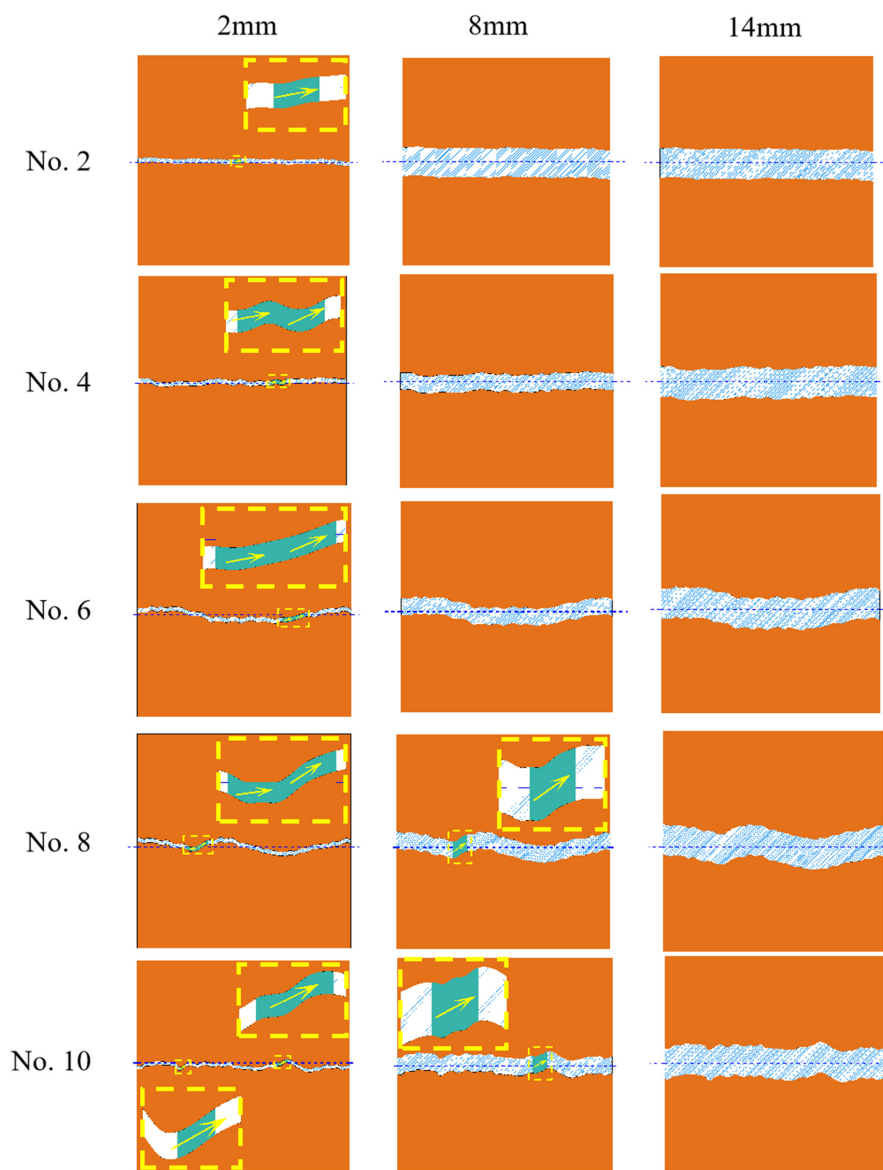
311 **Figure 12.** The shear rupture characteristics of ice-filled joints with different openings. Experimental condition: $T =$
312 $-5\text{ }^{\circ}\text{C}$, $d = 2\text{ mm}$ and $\sigma_n = 0.5\text{ MPa}$. The yellow lines show the main aggregation of rupture ice. Ice after rupture will
313 aggregate in roughness bulges perpendicular to the shear direction. The aggregation phenomenon disappears as the
314 joint openings increase. The aggregation phenomenon of profiles No. 2, No. 4 and No. 6 disappear in 8 mm joint
315 openings. All profiles' aggregation phenomena disappear in 14 mm joint openings.



316

317 **Figure 13.** Effect of joint opening on the peak shear strength. Experimental condition: $T = -5\text{ }^\circ\text{C}$, $v = 0.2\text{ mm/min}$

318 and $\sigma_n = 0.5\text{ MPa}$.

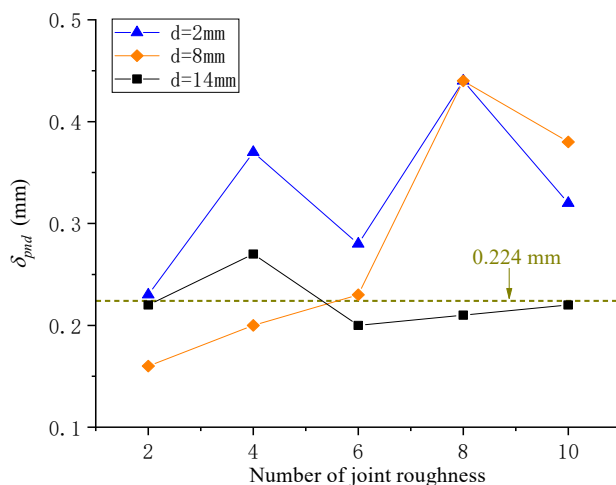


319

320 **Figure 14.** Influence of joint roughness on the shearing slip path. Experimental condition: $T = -5\text{ }^{\circ}\text{C}$, $v = 0.2\text{ mm/min}$

321 and $\sigma_n = 0.5\text{ MPa}$.

322



323

324 **Figure 15.** Effect of joint opening on the shearing dilatancy. Experimental condition: $T = -5\text{ }^{\circ}\text{C}$, $v = 0.2\text{ mm/min}$ and
 325 $\sigma_n = 0.5\text{ MPa}$.

326 3.5 Effect of normal stress

327 The normal stress group was used to investigate the effect of normal stress on the shear strength of ice-
 328 filled joints, including 0 MPa, 0.5 MPa, 1.0 MPa, 1.5 MPa and 2.0 MPa. The shear strength of ice-filled
 329 joints displays a significant increasing trend with increasing normal stress (Fig. 16). The Mohr-coulomb
 330 criterion may be used to express the relationship between the shear strength and normal stress as below:

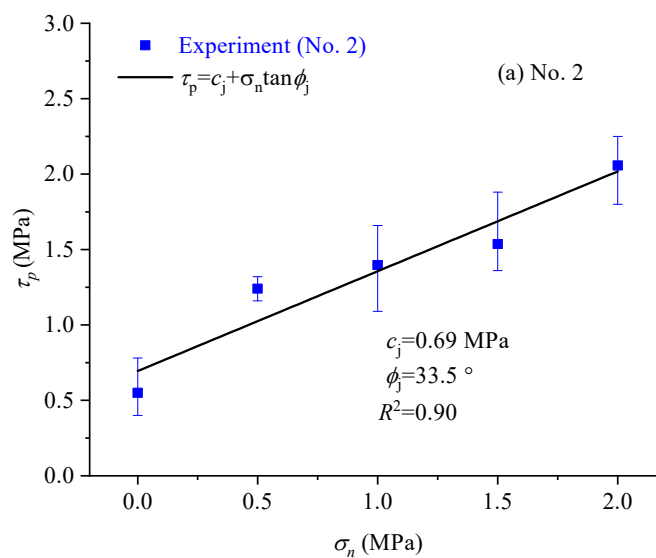
$$331 \tau_p = c_j + \sigma_n \tan \phi_j \quad (1)$$

332 Where τ_p = shear stress on plane, σ_n = normal stress on plane, c_j = cohesion of ice-filled joints,
 333 ϕ_j = internal friction angle of ice-filled joints.

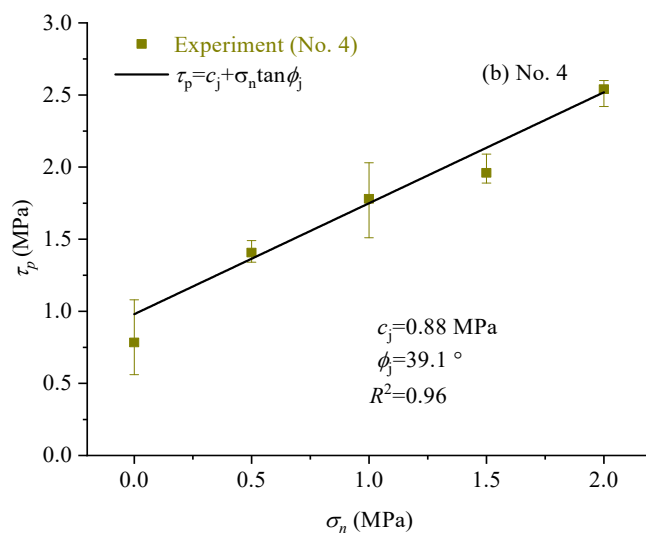
334 Figure 16 shows Mohr-coulomb criterion can be well used to calculate the shear strength of ice-filled
 335 joints against the normal stress. The shear rupture modes of the joint ice are given in Fig. 17. A
 336 remarkable ice aggregation phenomenon can be found on the surface of joints and the aggregation occurs



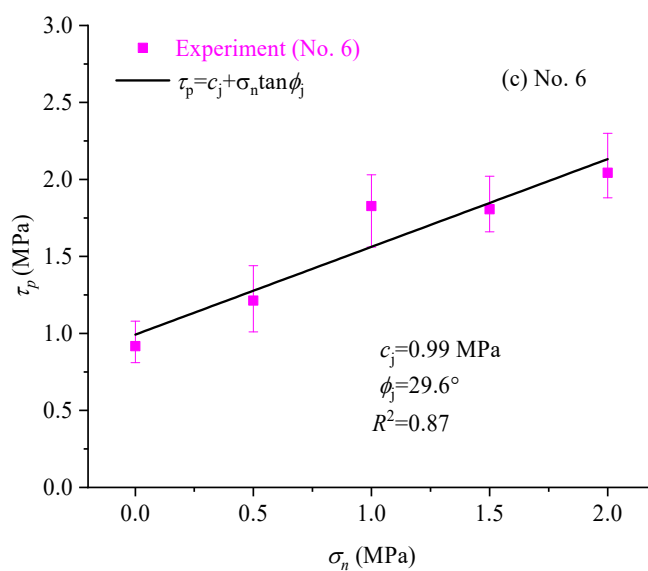
337 at a stable location of the joint profile regardless of the normal stress. The aggregation area of rupture ice
338 increases with increasing normal stress, because climbing bulges is harder and the solid ice is easier to
339 be crush at the front of large bulges under the higher normal stress (Fig. 18). In Section 3.1, it has
340 illustrated that the aggregation area of rupture ice is an important index to reflect the shear strength of
341 ice-filled joints at different freezing temperatures. Actually, the shear strength also linearly increases
342 with increasing the aggregation area of rupture ice under different normal stress as shown in Fig. 19. It
343 further illustrates that only some large bulges causing the aggregation of rupture ice can contribute to the
344 improvement of shear strength instead of the total roughness index, such as JRC.



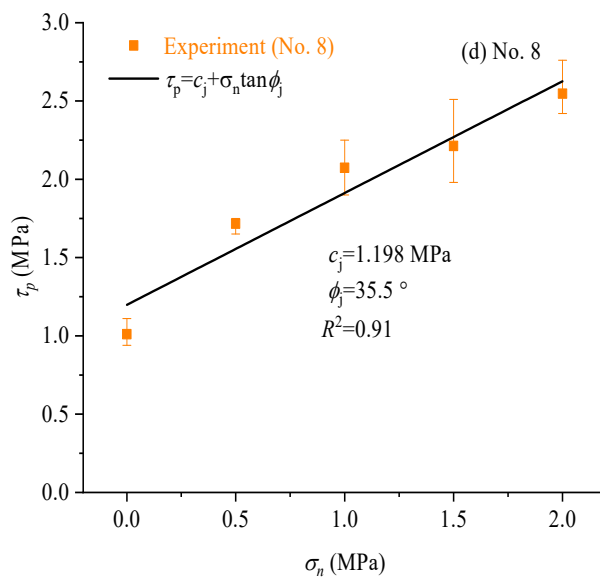
345



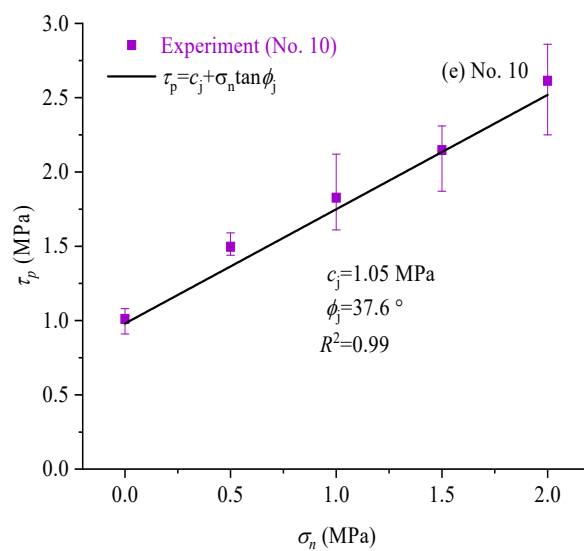
346



347



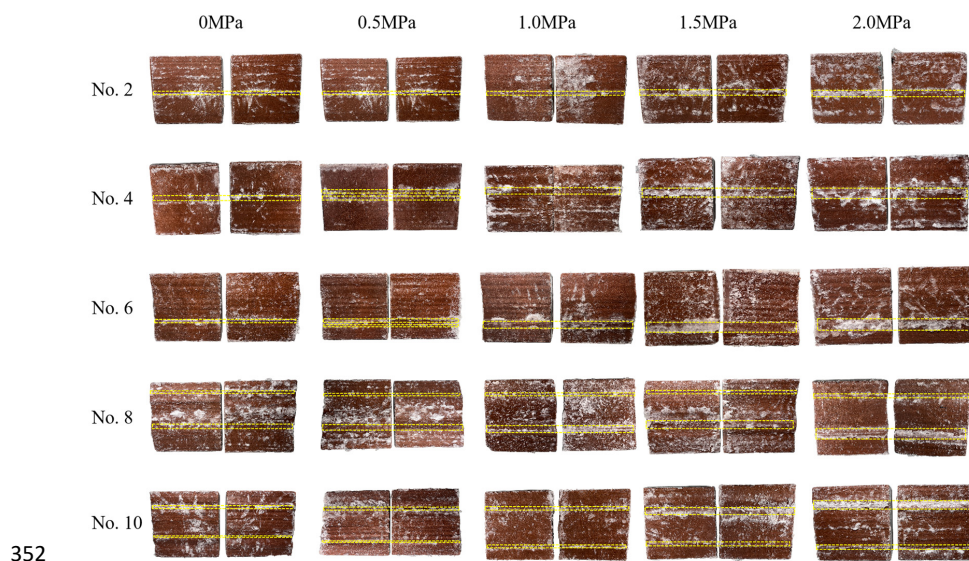
348



349

350 **Figure 16.** Effect of normal stress on the peak shear strength of ice-filled joints. Experimental condition: $T = -15^\circ\text{C}$,

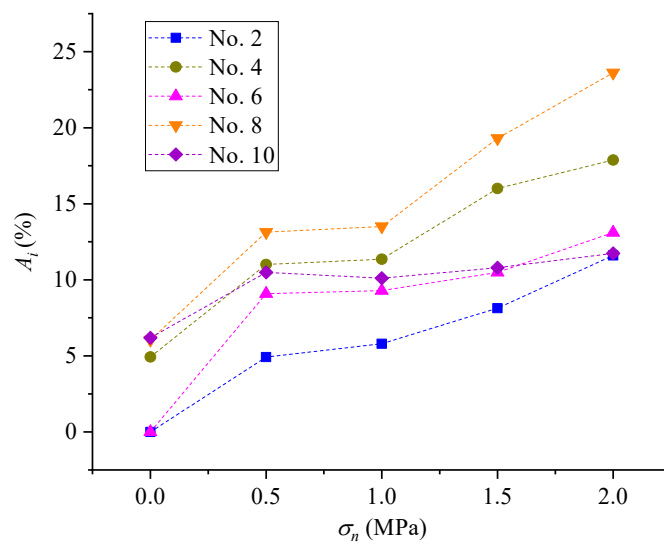
351 $v = 0.2 \text{ mm/min}$ and $\sigma_n = 0.5 \text{ MPa}$.



352

353 **Figure 17.** Aggregation of rupture ice under different normal stresses. Experimental condition: $T = -15\text{ }^{\circ}\text{C}$, $d = 2$

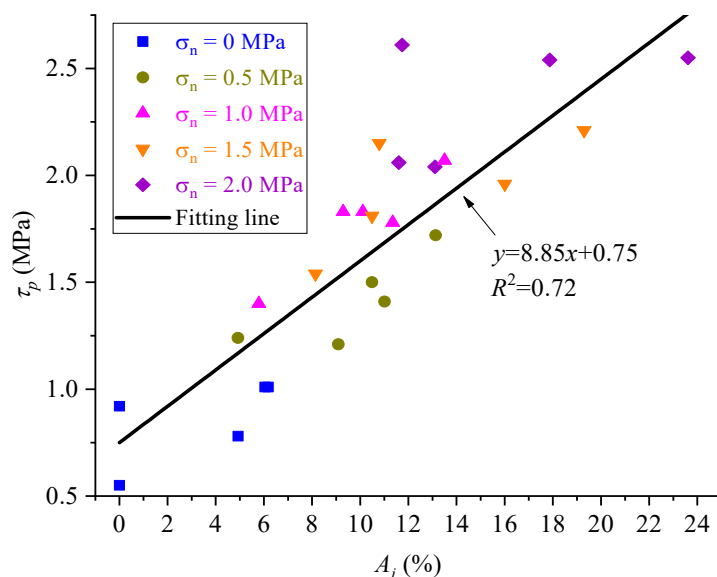
354 mm and $v = 0.2\text{ mm/min}$. The yellow lines show the main aggregation of rupture ice.



355

356 **Figure 18.** Aggregation area of rupture ice increases with increasing normal stress. Experimental condition: $T = -$

357 $15\text{ }^{\circ}\text{C}$, $d = 2\text{ mm}$ and $v = 0.2\text{ mm/min}$.



358

359 **Figure 19.** Peak shear strength linearly increases with increasing aggregation areas of rupture ice. Experimental

360 condition: $T = -15\text{ }^\circ\text{C}$, $d = 2\text{ mm}$ and $v = 0.2\text{ mm/min}$.

361 4. Discussion

362 4.1 The warming degradation mechanism of ice-filled joints

363 In this paper, the influence of freezing temperature, shear rate, joint opening and normal stress on the

364 shear strength of ice-filled joints in rock masses was comprehensively investigated by experiments. The

365 shear strength remarkably reduces with increasing freezing temperature, because the shear strengths of

366 solid ice and ice-rock interface decrease with increasing temperature. In order to deeply understand the

367 warming degradation mechanism of ice-filled joints, the shear strength of pure ice and ice-rock bonding

368 interface under different freezing temperatures also were tested in this study (Fig. 20).



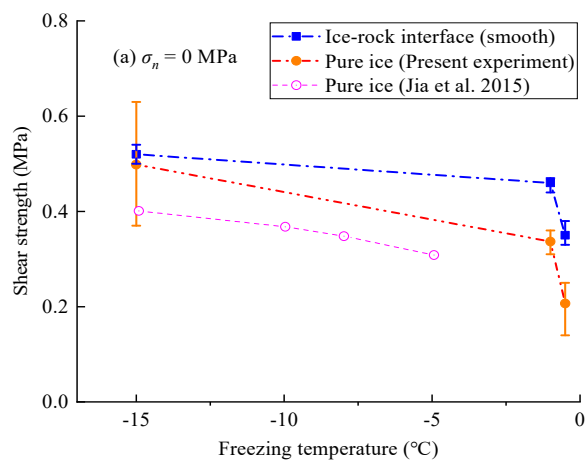
369 The test results show that the shear strength of smooth ice-rock bonding interface is larger than that of
370 pure solid ice at the freezing temperature from -15 to -0.5 °C (Fig. 20a). It implies that the shear failure
371 should be inside the solid ice instead of ice-rock interface. When the freezing temperature increase from
372 -1 °C to -0.5 °C, the shear strengths of the ice-rock interface and the solid ice reduce very quickly. Jia et
373 al. (2015) also claimed the same change law of solid ice against the temperature.

374 However, the experimental results show that the shearing failure of many rough ice-filled joints at -0.5 °C
375 is the debonding of ice-rock interfaces (Figs. 5, 11, 12, 17). More shear experiments were carried out on
376 rough ice-rock interfaces with profiles of No. 4 and No. 8 on the same experimental condition ($\sigma_n = 0.5$
377 MPa, $v = 0.2$ mm/min). It shows that the shear strength of rock-ice-rock “sandwich” is a little larger than
378 that of ice-rock interface, although the change laws of them against temperature are very similar. Another
379 novel finding is that the shear strength of ice-rock interface is larger than the shear strength of solid ice
380 itself below -1 °C (Fig. 20b). Therefore, the shear failure below -1 °C displays the cracking of joint ice
381 instead of ice-rock interface, and some aggregation areas of rupture ice occur before large bulges (Figs.
382 5, 11, 12, 17). However, the shear strength of solid ice is larger than that of ice-rock interface above -
383 1 °C. This is the main reason for the shear failure of rough ice-filled joints along ice-rock interfaces at -
384 0.5 °C. The freezing temperature of -1 °C is the transition point of shear failure modes. Figure 21 presents
385 that the shear failure is along the ice-rock interface when the freezing temperature is approximate -0.5 °C,
386 however, the area of ice attached to the joints has a great increment with the decrement of freezing
387 temperature from -0.5 °C to -15 °C. It further illustrates that the shear strength of rough ice-rock interface
388 is larger than that of the solid ice below -5°C. Mamot et al. (2018) also found that the shear failure modes
389 of the smooth ice-filled joints changed from shearing cracking of joint ice to the debonding of ice-rock



390 interface when the freezing temperatures increased from -10 °C to -0.5 °C. The smooth joints have a little
391 ability to resist the shear slide of ice-filled joints. Mamot et al. (2018) claimed that three shear failure
392 modes may arise between -5 °C to -1 °C, including the debonding of ice-rock interface, shear cracking
393 of joint ice and their mixed mode. However, only the shear cracking of joint ice occurs at -5 °C to -1 °C
394 in this study. Therefore, the joint roughness has an effect on the shear strength of ice-filled joints and the
395 shear failure modes.

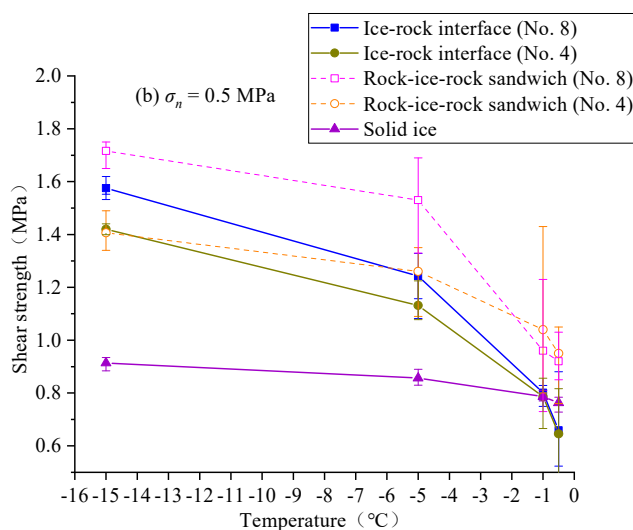
396



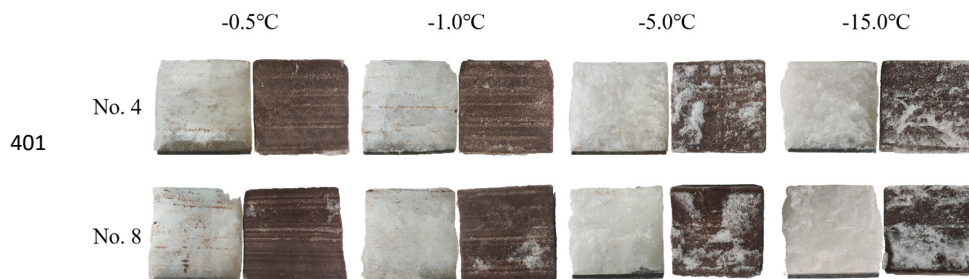
397



398



399 **Figure 20.** Influence of freezing temperature on the direct shear strength of ice and ice-filled joints. Experimental
 400 condition: $v = 0.2$ mm/min.



402 **Figure 21.** Shear failure characteristics of ice-rock interfaces under different temperatures. Experimental condition:
 403 $v = 0.2$ mm/min, $\sigma_n = 0.5$ MPa.

404

405 4.2 The coupled effect of joint roughness, opening and normal stress

406 The shear strength of smooth ice-filled joints were investigated by Mamot et al. (2018). They found that
 407 the shear strength of smooth ice-filled joints also linearly increases with decreasing temperatures.

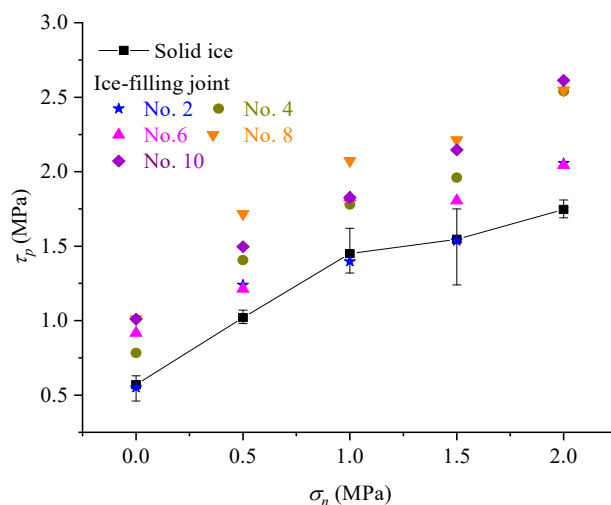


408 Actually, the roughness is another important factor influencing the shear strength of ice-filled joints,
409 which can improve the ability to resist the shear slide of joints (Fig. 22). The shear strength of the No. 2
410 ice-filled joint is much smaller than that of No. 8 and No. 10 joints. For the profile of No. 2, the shear
411 strength of ice-filled joint is approximately equal to that of the solid ice when the normal stress is less
412 than 1.5 MPa, because the joint opening of 2 mm also is very close to the maximum height difference.
413 Therefore, the joint opening will determine the effect of joint roughness. However, the shear strength of
414 solid ice is much smaller compared with the shear strength of ice-filled joints when the normal stress is
415 2 MPa. It is observed that this normal stress has caused some vertical micro-cracks inside the solid ice.
416 For the ice-filled joints, the compression damage maybe not remarkable, because both the adhesion of
417 ice-rock interface and bulges will prevent the lateral expansion of solid ice under high normal stress. A
418 larger roughness may provide a much stronger confining effect on the lateral expansion. Although the
419 shear strength increases with increasing JRC number in general, the quantitative relationship between
420 them are hard to determine. Figure 4 shows that the change of shear strength against the JRC number is
421 fluctuating. A novel finding of this study is that the aggregation area of rupture ice before large bulges
422 can be well used to predict the shear strength of ice-filled joints. However, it should be noted that a new
423 index of roughness should be proposed in future research in order to build the shear strength model
424 considering joint roughness.

425 In addition, if the joint opening exceeds the critical value, the influence of joint roughness on the shear
426 strength of ice-filled joints will disappear. For example, when the thickness of joint ice exceeds 14 mm,
427 the shear strength of all the ice-filled joints is equal to the shear strength of infilling ice. Section 3.4 has



428 illustrated that the value of critical joint opening is depended on the maximum height different of the
429 joint, which need to study further.



430
431 **Figure 22.** Shear failure characteristics of ice-rock interfaces under different normal stress. Experimental condition:
432 $v = 0.2\text{mm/min}$, $d = 2\text{ mm}$, $T = -15\text{ }^\circ\text{C}$.

433

434 4.3 Potential application for prediction of rock avalanches in a warming climate

435 In recent years, there are many large rock avalanches occurred in the Alps. The rock avalanches that
436 occurred on the Brenva gâlcier, the Punta Thurwieser and the Drus are some of the recent examples,
437 which have strong impacts on the high mountain infrastructure stability and landscape evolution (Mamot
438 et al., 2018). The rock avalanches are related to the degradation of bedrock permafrost and ice-filled
439 joints. Our study shows that the peak shear strength of ice-filled joints increases with the increase of
440 roughness and normal pressure. This implies that the rockfall will be more stable with higher roughness
441 and normal pressure. In addition, when the joint openings increase, the peak shear strength will decrease,



442 and large joint openings will reduce the effect of joint roughness. The peak shear strength of ice-filled
443 joints decreases with the increase of freezing temperature. Moreover, when the freezing temperature is
444 close to 0 °C, the pre-melting of ice-rock interface induced by the normal stress will cause a reduction of
445 bonding strength. This result can explain the phenomenon that the boundary of ice-filled joint between
446 frozen and unfrozen become unstable, especially in summer. The peak shear strength of ice-filled joints
447 decreases with the increase of shear rate. It is hard for the ice crystal to adjust to adapt the shear slip at
448 high shear rates so the rockfall may happen.

449 As the global temperature rises, collapse disasters of ice-filled rock mass caused by warming and thawing
450 often occur in permafrost regions. A constitutive model can be further constructed according to the
451 experiment results. Then combining with a numerical software, this constitutive model can be used to
452 predict the disaster of rock avalanches in the cold region in the future research. Although Mamot et al.
453 (2018) has established a constitutive model for joints, the constitutive model only considers temperature
454 and normal stress, however, the influence of the joint roughness, opening and shear rate is ignored.
455 Through our study, it is evidenced that the joint roughness, shear rate, joint opening and temperature are
456 physical quantities that must be considered in the constitutive model. A constitutive model including
457 these physical quantities will be proposed in our future research.

458 **5 Conclusions**

459 Above all, this study has provided a comprehensively experimental study on the shear process of ice-
460 filled joints, considering the influence of freezing temperature, joint roughness, shear rate, joint opening
461 and normal stress. The following conclusions can be drawn based on this research:



462 (1) The shear strength of ice-filled joints decreases with increasing temperature. The shear failure mode
463 change from shear cracking of joint ice to the debonding of ice-rock interface when the temperature
464 increases to $-0.5\text{ }^{\circ}\text{C}$, because the bonding strength of ice-rock interface is less than that of solid ice at -
465 $0.5\text{ }^{\circ}\text{C}$ ($v = 0.2\text{mm/min}$, $\sigma_n = 0.5\text{ MPa}$).

466 (2) The joint roughness can improve the shear strength of ice-filled joints. The shear strength of ice-filled
467 joints linearly increases with increasing the aggregation area of rupture ice before some large bulges.
468 However, the relationship between the JRC index and the shear strength is poor. In addition, the effect
469 of joint roughness is related to the joint opening and normal stress.

470 (3) The shear strength of ice-filled joints decreases with increasing joint opening. When the joint opening
471 increases from 2 mm to 14 mm, the aggregation of rupture gradually disappears and the shear strength
472 of ice-filled joint is equal to that of solid ice. Therefore, the joint roughness does not make any
473 contribution to the shear strength when the joint opening exceeds a critical value, which is related to the
474 maximum height difference of joint surface.

475 (4) The shear strength of ice-filled joints decreases when the shear rate increase from 0.2 mm/min to 0.8
476 mm/min. The infilling ice will change from ductile failure to brittle failure by observing the rupture ice
477 on the joint surface. The aggregation area of rupture ice also decreases while the brittle rupture
478 phenomenon is more serious with increasing shear rate.

479 (5) The shear strength of ice-filled joints linearly increases with increasing normal stress, which well
480 satisfies the Mohr-coulomb criterion. The aggregation area of rupture ice also increases with increasing
481 normal stress. In addition, the improvement of shear strength of the ice-filled joints caused by normal



482 stress is much larger than that of solid ice, because the bulges of the joint surface can prevent the lateral
483 expansion of ice under compression.

484 **Acknowledgements**

485 This work was supported by National Natural Science Foundation of China (Grant No. 42072300 and
486 No. 41702291), Project of Natural Science Foundation of Hubei Province (Grant No. 2021CFA094).

487 **Conflict of interest**

488 The authors declared that they have no conflicts of interest to this work.

489 **Reference**

490 Allen, S. and Huggel, C.: Extremely warm temperatures as a potential cause of recent high mountain
491 rockfall, *Global. Planet. Change.*, 107, 59-69, <https://doi.org/10.1016/j.gloplacha.2013.04.007>, 2013.

492 Barton, N. and Choubey, V.: The shear strength of rock joints in theory and practice, *J. Rock. Mech.*
493 *Geotech.*, 10, 1-54, <https://doi.org/10.1007/BF01261801>, 1977.

494 Bragov, A., Igumnov, L., Konstantinov, A., Lomunov, A., Filippov, A., Shmotin, Y., Didenko R. and
495 Krundaeva, A.: Investigation of strength properties of freshwater ice, *EPJ Web of Conferences.*, 94,
496 01070, <https://doi.org/10.1051/epjconf/20159401070>, 2015.

497 Colucci, R. R. and Guglielmin, M.: Climate change and rapid ice melt: Suggestions from abrupt
498 permafrost degradation and ice melting in an alpine ice cave, *Prog. Phys. Geog.*, 43, 561-573,
499 <https://doi.org/10.1177/0309133319846056>, 2019.



- 500 Davies, M. C., Hamza, O. and Harris, C.: The effect of rise in mean annual temperature on the stability
501 of rock slopes containing ice-filled discontinuities, *Permafrost. Periglac.*, 12, 137-144,
502 <https://doi.org/10.1002/ppp.378>, 2001.
- 503 Davies, M. C., Hamza, O., Lumsden, B. W. and Harris, C.: Laboratory measurement of the shear strength
504 of ice-filled rock joints, *Ann. Glaciol.*, 31, 463-467, <https://doi.org/10.3189/172756400781819897>, 2017.
- 505 Etzelmüller, B., Czekirda, J., Magnin, F., Duvillard, P. A., Raveland, L., Malet, E., Aspaas A., Kristensen
506 L., Skrede I., Majala G. D., Jacobs B., Leinauer J., Hauck C., Hilbich C., Böhme M., Hermanns R.,
507 Eriksen H., Lauknes T. R., Krautblatter M. and Westermann, S.: Permafrost in monitored unstable rock
508 slopes in Norway—new insights from temperature and surface velocity measurements, geophysical
509 surveying, and ground temperature modelling, *Earth. Surf. Dynam.*, 10, 97-129,
510 <https://doi.org/10.5194/esurf-10-97-2022>, 2022.
- 511 Gold, L. W.: Engineering properties of fresh-water ice, *J. Glaciol.*, 19, 197-212,
512 <https://doi.org/10.3189/S0022143000215608>, 2018.
- 513 Gruber, S. and Haeberli, W.: Permafrost in steep bedrock slopes and its temperature-related
514 destabilization following climate change, *J. Geophys. Res.-Earth.*, 112, F02S18,
515 <https://doi.org/10.1029/2006JF000547>, 2007.
- 516 Han, H. W., Jia, Q., Huang, W. F. and Li, Z. J.: Flexural strength and effective modulus of large
517 columnar-grained freshwater ice, *J. Cold. Reg. Eng.*, 30, 04015005,
518 [https://doi.org/10.1061/\(ASCE\)CR.1943-5495.0000098](https://doi.org/10.1061/(ASCE)CR.1943-5495.0000098), 2016.



- 519 Hartmeyer, I., Delleske, R., Keuschnig, M., Krautblatter, M., Lang, A., Schrott, L. and Otto, J. C.: Current
520 glacier recession causes significant rockfall increase: the immediate paraglacial response of deglaciating
521 cirque walls, *Earth. Surf. Dynam.*, 8, 729-751, <https://doi.org/10.5194/esurf-8-729-2020>, 2020.
- 522 Hilger, P., Hermanns, R. L., Czekirda, J., Myhra, K. S., Gosse, J. C. and Etzelmüller, B.: Permafrost as
523 a first order control on long-term rock-slope deformation in (Sub-) Arctic Norway, *Quaternary. Sci. Rev.*,
524 251, 106718, <https://doi.org/10.1016/j.quascirev.2020.106718>, 2021.
- 525 Krautblatter, M., Funk, D., Günzel, F. K.: Why permafrost rocks become unstable: a rock-ice-mechanical
526 model in time and space, *Earth. Surf. Proc. Land.*, 38, 876-887, <https://doi.org/10.1002/esp.3374>, 2012.
- 527 Krautblatter, M., Huggel, C., Deline, P. and Hasler, A.: Research perspectives on unstable high-alpine
528 bedrock permafrost: Measurement, modelling and process understanding, *Permafrost. Periglac.*, 23, 80-
529 88, <https://doi.org/10.1002/ppp.740>, 2021.
- 530 Legay, A., Magnin, F. and Ravel, L.: Rock temperature prior to failure: Analysis of 209 rockfall events
531 in the Mont Blanc massif (Western European Alps), *Permafrost. Periglac.*, 32, 520-536,
532 <https://doi.org/10.1002/ppp.2110>, 2021.
- 533 Luo, S., Li, C., Li, F., Wang, J. and Li, Z. G.: Ice crystallization in shear flows, *J. Phys. Chem. C.*, 123,
534 21042-21049, <https://doi.org/10.1021/acs.jpcc.9b06225>, 2019.
- 535 Mamot, P., Weber, S., Eppinger, S. and Krautblatter, M.: A temperature-dependent mechanical model to
536 assess the stability of degrading permafrost rock slopes, *Earth. Surf. Dynam.*, 9, 1125-1151,
537 <https://doi.org/10.5194/esurf-9-1125-2021>, 2021.



- 538 Mamot, P., Weber, S., Schröder, T. and Krautblatter, M.: A temperature-and stress-controlled failure
539 criterion for ice-filled permafrost rock joints, *Cryosphere.*, 12, 3333-3353, [https://doi.org/10.5194/tc-12-](https://doi.org/10.5194/tc-12-3333-2018)
540 3333-2018, 2018.
- 541 Matsuoka, N. and Murton, J.: Frost weathering: recent advances and future directions, *Permafrost.*
542 *Periglac.*, 19, 195-210, <https://doi.org/10.1002/ppp.620>, 195-210.
- 543 Petrovic, J. J.: Review mechanical properties of ice and snow, *J. Mater. Sci.*, 38, 1-6,
544 <https://doi.org/10.1023/A:1021134128038>, 2003.
- 545 Schulson, E. M. and Fortt, A. L.: Friction of ice on ice, *J. Geophys. Res.-Sol. Ea.*, 117, B12204,
546 <https://doi.org/10.1029/2012JB009219>, 2012.
- 547 Shan, R. L., Bai, Y., Ju, Y., Han, T. Y., Dou, H. Y. and Li, Z. L.: Study on the triaxial unloading creep
548 mechanical properties and damage constitutive model of red sandstone containing a single ice-filled flaw,
549 *Rock. Mech. Rock. Eng.*, 54, 833-855, <https://doi.org/10.1007/s00603-020-02274-1>, 2021.
- 550 Shen, Y. J., Yang, H. W., Xi, J. M., Yang, Y., Wang, Y. Z. and Wei, X.: A novel shearing fracture
551 morphology method to assess the influence of freeze-thaw actions on concrete-granite interface, *Cold.*
552 *Reg. Sci. Technol.*, 169, 102900, <https://doi.org/10.1016/j.coldregions.2019.102900>, 2020.
- 553 Shugar, D. H., Jacquemart, M., Shean, D., Bhushan, S., Upadhyay, K., Sattar, A., Schwanghart, W.,
554 McBride, S., Van Wyk De Vries, M., Mergili, M., Emmer, A., Deschamps-Berger, C., McDonnell, M.,
555 Bhabri, R., Allen, S., Berthier, E., Carrivick, J. L., Clague, J. J., Dokukin, M., Dunning, S. A., Frey,
556 H., Gascoin, S., Haritashya, U. K., Huggel, C., Kääh, A., Kargel, J. S., Kavanaugh, J. L., Lacroix, P.,



- 557 Petley, D., Rupper, S., Azam, M. F., Cook, S. J., Dimri, A. P., Eriksson, M., Farinotti, D., Fiddes, J.,
558 Gnyawali, K. R., Harrison, S., Jha, M., Koppes, M., Kumar, A., Leinss, S., Majeed, U., Mal, S., Muhuri,
559 A., Noetzli, J., Paul, F., Rashid, I., Sain, K., Steiner, J., Ugalde, F., Watson, C. S. and Westoby, M. J.: A
560 massive rock and ice avalanche caused the 2021 disaster at Chamoli, Indian Himalaya, *Science.*, 373,
561 300-306, 10.1126/science.abh4455, 2021.
- 562 Sinha, N. K.: Elasticity of natural types of polycrystalline ice, *Cold. Reg. Sci. Technol.*, 17, 127-135,
563 [https://doi.org/10.1016/S0165-232X\(89\)80003-5](https://doi.org/10.1016/S0165-232X(89)80003-5), 1989.
- 564 Timco, G. W. and Frederking, R. M. W.: Comparative strengths of fresh water ice, *Cold. Reg. Sci.*
565 *Technol.*, 6, 21-27, [https://doi.org/10.1016/0165-232X\(82\)90041-6](https://doi.org/10.1016/0165-232X(82)90041-6), 1982.
- 566 Walter, F., Amann, F., Kos, A., Kenner, R., Phillips, M., de Preux, A., Huss, M., Tognacca, C., Clinton,
567 J., Diehl, T. and Bonanomi, Y.: Direct observations of a three million cubic meter rock-slope collapse
568 with almost immediate initiation of ensuing debris flows, *Geomorphology.*, 351, 106933,
569 <https://doi.org/10.1016/j.geomorph.2019.106933>, 2019.
- 570 Weber, S., Fäh, D., Beutel, J., Failletaz, J., Gruber, S. and Vieli, A.: Ambient seismic vibrations in steep
571 bedrock permafrost used to infer variations of ice-fill in fractures, *Earth. Planet. Sc. Lett.*, 501, 119-127,
572 <https://doi.org/10.1016/j.epsl.2018.08.042>, 2018.
- 573 Yang, Q. Q., Su, Z. M., Cheng, Q. G., Ren, Y. H. and Cai, F.: High mobility of rock-ice avalanches:
574 Insights from small flume tests of gravel-ice mixtures, *Eng. Geol.*, 260, 105260,
575 <https://doi.org/10.1016/j.enggeo.2019.105260>, 2019.



576 Zhang, G. Z., Chen, G. Q., Xu, Z. X., Yang, Y. and Lin, Z. H.: Crack failure characteristics of different
577 rocks under the action of frost heaving of fissure water, *Front. Earth. Sc.-Switz.*, 8, 13,
578 <https://doi.org/10.3389/feart.2020.00013>, 2020.

579 Zhao, Z. H., Yang, J., Zhou, D. and Chen, Y. F.: Experimental investigation on the wetting-induced
580 weakening of sandstone joints, *Eng. Geol.*, 225, 61-67, <https://doi.org/10.1016/j.enggeo.2017.04.008>,
581 2017.